Clustering of Cyclic-Nucleotide-Gated Channels in Olfactory Cilia

Richard J. Flannery,* Donald A. French,[†] and Steven J. Kleene*
*Department of Cell Biology, Neurobiology, and Anatomy, and [†]Department of Mathematical Sciences, University of Cincinnati, Cincinnati, Ohio

ABSTRACT   Olfactory cilia contain the known components of olfactory signal transduction, including a high density of cyclic-nucleotide-gated (CNG) channels. CNG channels play an important role in mediating odor detection. The channels are activated by cAMP, which is formed by a G-protein-coupled transduction cascade. Frog olfactory cilia are 25–200 μm in length, so the spatial distribution of CNG channels along the length should be important in determining the sensitivity of odor detection. We have recorded from excised cilia and modeled diffusion of cAMP into a cilium to determine the spatial distribution of the CNG channels along the ciliary length. The proximal segment, which in frog is the first 20% of the cilium, appears to express a small fraction of the CNG channels, whereas the distal segment contains the majority, mostly clustered in one region.

INTRODUCTION

Olfactory signal transduction occurs on the olfactory cilia, which extend from the tip of the dendritic knob of each olfactory receptor neuron (1). The cilia contain molecules required for transduction of an odor stimulus, including odorant receptor proteins, the G-protein G_{olf}, adenylate cyclase III, cAMP phosphodiesterase, and two transduction channels (1,2). One of these, a cyclic-nucleotide-gated (CNG) channel, is gated by cAMP and conducts a depolarizing cationic current into the cilium. CNG channels are expressed at high densities in olfactory cilia (3–6). Cilia increase the neuron's ability to detect odor molecules by extending into the mucus and by increasing the surface area of the sensory neuron by as much as 40 times (2). In frog, a cilium's length is on the order of 100 times its diameter. This geometry may be ideal for increasing binding of odor molecules to the surface, but it may also lead to unique challenges for transducing signals after an odor molecule binds. A consequence of the extreme geometry is that second messengers may need to diffuse over considerable distances (7). It has been shown in other cell types that cAMP and CNG channels interact within and are restricted to domains, thus limiting the distance over which cAMP must diffuse (8,9).

The distribution of CNG channels along the length of the cilium should be an important determinant of neuronal sensitivity. However, this distribution is uncertain. An electrophysiological study in salamander suggested that the channels might be uniformly distributed along the length of the cilium (10). Immunohistochemical studies of channels in rat olfactory cilia indicated that channels are expressed more prominently in distal regions (11). Existing models of olfactory neuron function assume that ion channels are distributed uniformly (4,5,7,12,13).

We have applied a computational model to patch-clamp experiments to determine the locations of the CNG channels along the ciliary length. Our results show that the distal segment contains the majority of the CNG channels, and these channels tend to be clustered in one region.

METHODS

Ciliary patch procedure

Electrical recordings were made from olfactory cilia of Northern grass frogs (*Rana pipiens*) as described elsewhere (14). Frog olfactory epithelium was dissociated by mechanical shredding. One cilium of an isolated olfactory receptor neuron was drawn into a patch pipette, and a high-resistance seal was made where the olfactory knob meets the base of the cilium. The cilium was then excised from the cell, resulting in an inside out patch configuration. The pipette containing the cilium was moved to a pseudointracellular bath so that the intracellular side of the cilium was exposed to the bath solution.

This first pseudointracellular bath contained no cAMP. The leak current measured in this bath was subtracted from all subsequent measurements. The leak current averaged -28 ± 1 pA ($n = 90$). The pipette containing the cilium was then transferred through the air to a bath containing cAMP. Contact with the bath initiated the diffusion of cAMP into the cilium (Fig. 1). The resulting CNG channel activation was recorded over a period of ~4 s. Maximal channel activity was typically achieved after ~1–2 s. The patch procedure was videotaped, and ciliary lengths were estimated by playing back the video images one frame at a time. Multiple tests were conducted with each cilium. Between tests, the cilium was placed in a cAMP-free bath for ~1 min, which was longer than the time required for the current to return to the leak value. This took from 2 to 19 s; longer times were required with longer cilia and higher concentrations of cAMP.

The extracellular (pipette) solution contained (in mM): NaCl, 115; KCl, 3; Na_3-EDTA, 1; Na-HEPES, 5; pH 7.2. The pseudointracellular (bath) solution contained (in mM): NaCl, 110; KCl, 5; K_4-BAPTA, 2; K-HEPES, 5; IBMX (3-isobutyl-1-methylxanthine), 0.1; pH 7.2. IBMX, a phosphodiesterase inhibitor, was included to reduce hydrolysis of cAMP. Both solutions were free of divalent cations. This eliminated the possibility that Ca^{2+} might enter the cilium and activate a Cl^- current (15,16). With these solutions, the cAMP-activated current reversed near 0 mV. For electrical recording, both the recording pipette and chamber were coupled to an Axopatch-1D patch-clamp amplifier by Ag/AgCl electrodes. All recordings were done under voltage-clamp at -50 mV at room temperature (25°C). Current was sampled at 250 or 500 Hz by pCLAMP 5.5 software (Axon Instruments/Molecular Devices, Union City, CA).
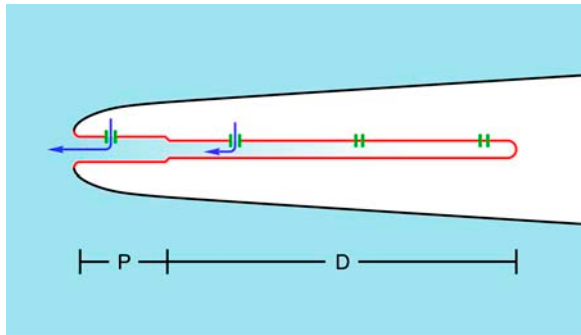
FIGURE 1 Schematic diagram of the experimental method. A single cilium (shown in *red*) from a frog olfactory receptor neuron is sealed inside a glass micropipette (*black*). The base of the cilium, which is attached to the dendrite in vivo, is shown at the left. The distal tip is at the right. The base of the cilium is open and allows diffusion of cAMP (*light blue*) from the surrounding bath into the cilium. As cAMP reaches CNG channels (*green*) in the ciliary membrane, it gates them, allowing an influx of Na^+ (*dark blue arrows*). The uniform distribution of channels shown does not represent the experimental finding. At the bottom are shown the approximate extents of the proximal (*P*) and distal (*D*) segments of the cilium as described by Reese (21). The schematic is not drawn to scale.

Modeling

Two versions of the biophysical model were employed in our study: a forward version and an inverse solution. The inverse solution was done first, generating a channel density function from an experimental record of current versus time. The accuracy of the density function was then assessed by using the density function as input for the forward model. The forward model makes predictions about the time course of the current through the CNG channels, given a channel density function. The predicted current was compared to the experimental result. The model easily discriminates between uniform and step distributions of channels (see French et al. (17) and Fig. 10). In all figures, 0 represents the proximal end of the cilium (i.e., the end that is close to the basal body).

Forward biophysical model

A computational model was used to make predictions about channel currents resulting from diffusion of cAMP into a cilium, given a particular ion channel density function (for example, see Fig. 3). The model accounted for several physical processes, including diffusion of cAMP, binding of cAMP to the CNG channels, channel activation, and cable-conduction effects. Diffusion and binding of cAMP were modeled by a nonlinear time-dependent partial differential equation that also depends on the channel distribution, $\rho(x)$. Activation of channels by cAMP was represented by a two-parameter Hill equation rather than by specifying the required number of binding events. Membrane potential satisfies a second-order boundary value problem that depends on ρ, the concentration of cAMP, and time. These equations are approximated by basic finite difference schemes. A detailed description of this model is given in French et al. (17).

Some minor factors were not included in the model. It does not account for a small leak conductance in the ciliary membrane (18). Only cilia with minimal leak conductance (input resistance ≥ 1 GΩ) were used. The model also assumes that the cilium is a cylinder of constant diameter. In fact, the diameter decreases abruptly from 0.28 μm to 0.19 μm where the proximal and distal segments meet (19). It is assumed that unhindered diffusion of cAMP is possible in the entire volume of the cilium and that this diffusion is not affected by the applied voltage (13). Binding of cAMP to the CNG channels is considered to be much faster than diffusion. Other possible membrane-associated cAMP-binding sites (e.g., cAMP phosphodiesterase)

were not modeled because quantitative data are unavailable. Finally, capacitative current has been ignored. We estimate that the time constant of a cilium should be ~3 ms, which is much faster than the events recorded here.

Inverse solution

The primary unknown in our biophysical model is the spatial distribution of the CNG channels, and it was the aim of our modeling and experiments to generate a function quantifying this unknown. The inverse solution offers a systematic way of generating density functions, using the measured time-dependent activation of CNG channels as input. The inverse solution has the same components as those described in the forward biophysical model, as well as a Fredholm integral equation that has a kernel that depends on the membrane potential and concentration of cAMP. Through a series of iterations, the inverse solution makes an approximation of the density function, $\rho(x)$. The inverse solution is described in greater detail in French et al. (17).

The noisy raw current data were smoothed by a moving average with 11 points and then used to generate an inverse solution (a channel density function ρ). For this approximation, the smoothed raw data were averaged over each of the $N = 20$ intervals of length T/N, where T is the duration of the recording. This yielded a piecewise constant current. To evaluate the inverse solution, the channel density function ρ was used to calculate a predicted current using the forward model. Using the piecewise constant ρ function, a discrete cAMP concentration and membrane potential were computed using finite differences. Discrete current values were then produced at the 21 nodal points in time. Where average density functions are shown, each point is a mean $\pm$ SE. When the average includes cilia tested more than once, each measurement is weighted equally.

Data selection and analysis

Of the density functions, ~70% were judged to be credible, and the remaining 30% were rejected. A given channel density function was rejected for either of two reasons. Some were rejected because the model reported an unrealistically high number of channels, often with all channels located at the proximal or distal end of the cilium. Based on an unpublished analysis of a study of 117 cilia (5), we rejected solutions that predicted >40,000 channels for a cilium. Other solutions were rejected because the measured and predicted currents did not match. The forward model should convert the inverse solution (a density function) to a current record the same as the experimental recording in every respect except noise (see Fig. 3 *A*). The sum of the absolute values of the differences between the predicted and true currents was divided by the area under the true current curve. We refer to this relative error as the residual value; if it was >0.35, we rejected the solution. After some practice, it was always possible to design a density function by trial and error such that providing the function as input to the forward model accurately predicted the experimental recording. However, all of the density functions shown were produced as inverse solutions rather than by trial and error.

In Figs. 5, 8, and 9, we compare channel density functions in a population of cilia of various lengths. For this purpose the length of each cilium was arbitrarily assigned a value of 100. Because the number of channels varies widely among cilia (5), we also normalized the number of channels when comparing different cilia. In such cases the sum of the heights of all of the bars shown is 1.

RESULTS

When a cilium was quickly lowered from the air into a bath containing cAMP, there was a short delay (a period of CNG current activation with a relatively shallow slope), after which the current increased more rapidly. For one 100-μm

cilium, the delay was 200 ms in 10 μM cAMP (Fig. 2 *A*) and 70 ms in 300 μM cAMP (Fig. 2 *B*). Longer delays were seen with longer cilia and lower [cAMP] (Table 1). Without regard to length of the cilium, the average delays in 10 μM cAMP and 300 μM cAMP were 78 and 39 ms, respectively.

After the delay, the cAMP-activated current increased rapidly, reaching a maximum after 200 ms or longer, again depending on [cAMP] and length of the cilium. The time to reach the maximum current was longer when longer cilia or lower [cAMP] were used. The maximum current amplitude was highly variable. There is no correlation between ciliary length and maximum current (5). In the model, the initial phase of current activation primarily determined the proximal channel patterns, whereas the slope of the second phase was the primary determinant for distal channel patterns.

One 70-μm cilium reached a maximum current of 100 pA after ~1 s (Fig. 3 *A*). Seven such experiments were performed with this cilium using cAMP concentrations of 10 or 20 μM. For each experiment, the inverse solution was used
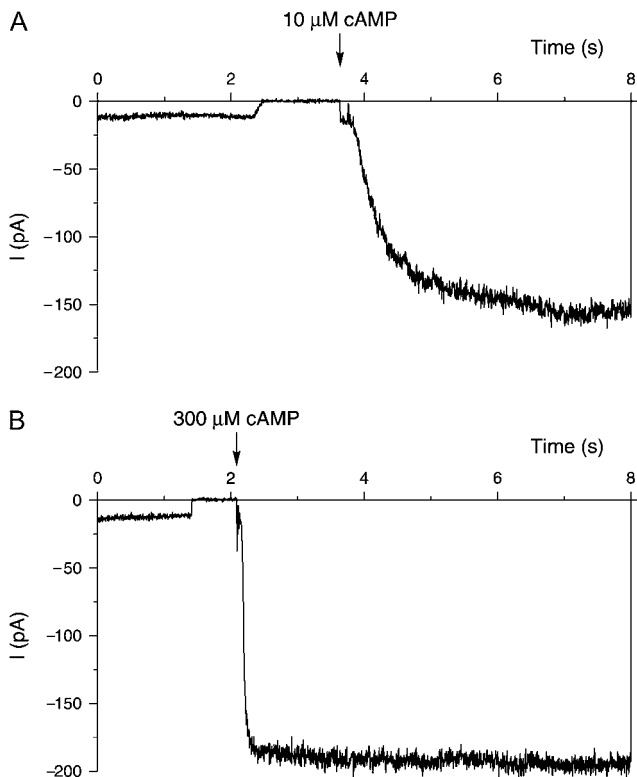
TABLE 1 Delays in activation of CNG current

Length of cilium	Current delay (ms)	
	[cAMP] = 10 μM	[cAMP] = 300 μM
40 μm	42 ± 9 (n = 6)	20 ± 5 (n = 6)
70 μm	52 ± 11 (n = 6)	22 ± 2 (n = 6)
100 μm	131 ± 11 (n = 7)	69 ± 4 (n = 7)

The time (as mean ± SE) is shown between immersion of the cilium in cAMP and the onset of the rapidly increasing current. Each row lists repeated measurements from a single cilium. To measure the delay, the leak current in the absence of cAMP was first measured (e.g., the initial part of each recording shown in Fig. 2, where the leak was −13 pA). The delay was the difference between the time the cilium was immersed in a cAMP-containing bath (*arrows* in Fig. 2) and the time when the current became more negative than the leak current. The first row is from the same cilium used for Fig. 2.

to generate a density function. Three of the density functions for this cilium are shown in Fig. 3 *B*, *D*, and *F*. These density functions have common features. Usually most of the channels were clustered in one small region 5–10 μm wide. This primary cluster appeared in density functions from most trials using the same cilium, regardless of cAMP concentration. In some individual trials (e.g., Fig. 3 *B*), additional smaller clusters appeared. When all seven density functions for this cilium were averaged (Fig. 4 *A*), the smaller clusters disappeared or appeared as shoulders in the main peak.

Averaged density functions for each of three cilia are shown in Fig. 4, *A–C*. In each averaged density function, there was one major cluster 10–15 μm wide in the distal segment. A smaller cluster appeared near the base of the cilium, and this cluster was more prominent in some cilia (e.g., Fig. 4 *C*). At least two concentrations of cAMP were used for each cilium. Typically these included a saturating dose, usually 20 μM, and a lower dose, between 1 and 10 μM.

The clustering of CNG channels was apparent even when density functions from 42 experiments in 13 cilia were averaged (Fig. 5 *A*). To facilitate comparisons among the cilia, ciliary length and number of channels were normalized. For this average density function, the distance from the base of the cilium to the peak of the density function was 28% of the length of the cilium. This should be in the distal segment of the cilium (Fig. 5 *B*).

FIGURE 2 Time courses of CNG current activated by placing a 100-μm cilium in 10 μM cAMP (*A*) and then 300 μM cAMP (*B*). At the start of each recording, the cilium was in a cAMP-free bath and showed a leak current of ~13 pA. The cilium was briefly moved through the air, during which time the current was 0 pA. At the time indicated by the arrow, the cilium was immersed in a bath containing cAMP. Initially, this activated a current with a slow rise and a very low amplitude (0–5 pA after subtraction of the leak current). This was followed by a current with a steeper slope that began ~200 ms (*A*) or 70 ms (*B*) after immersion in the cAMP-containing bath. Membrane potential was clamped at −50 mV throughout the experiment.

Accumulation of sodium

Our model assumes that the concentration of the current-carrying ion (Na^+) is equal and constant on both sides of the ciliary membrane. It was conceivable, though, that the influx of Na^+ during the experiment might cause an accumulation of Na^+ within the tiny volume of the cilium (20). To test this, voltage was applied instantaneously to a cilium already filled with a saturating concentration of cAMP. Maintaining this
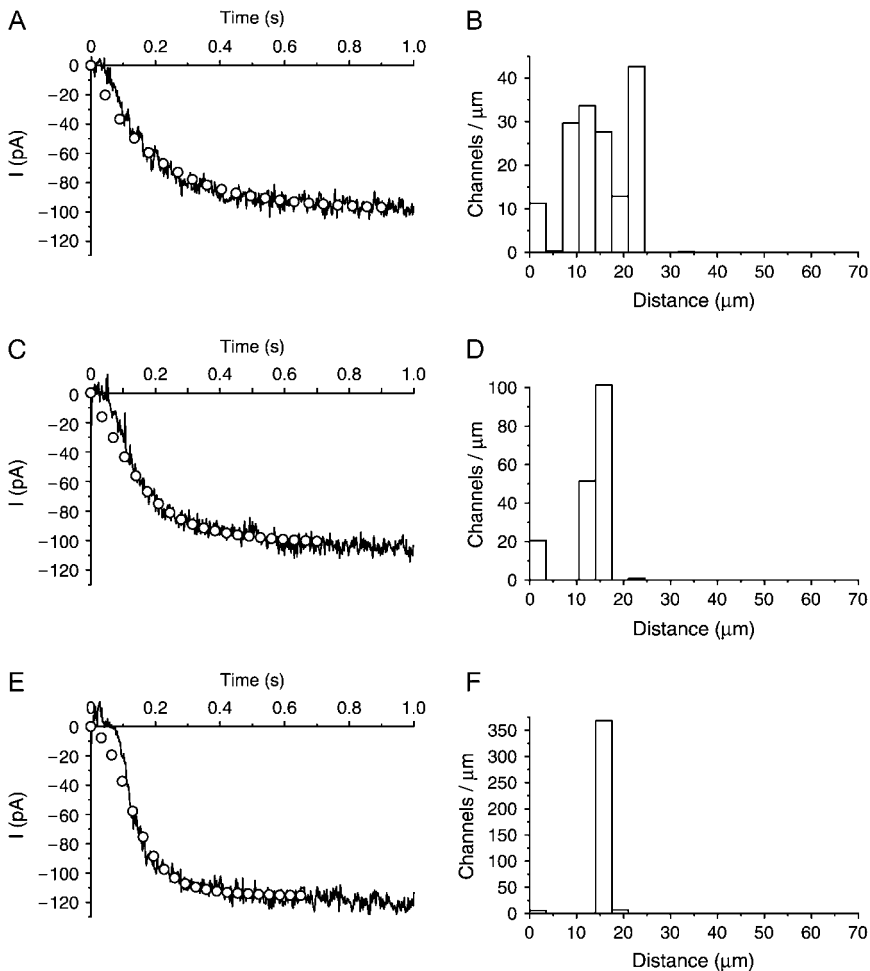
FIGURE 3 Density functions of CNG channels generated from electrical recordings in a single 70-μm cilium. (*A*) The continuous curve shows the current measured after the cilium was immersed in 10 μM cAMP. The leak current in a cAMP-free bath (-39 pA) has been subtracted. Given this recording, an inverse solution of the channel density function (*B*) was generated with the mathematical model. A forward calculation from this density function predicted the current shown as open circles in *A*. (*C–F*) show two additional trials with the same cilium. Leak currents were -33 pA and -32 pA for *C* and *E*, respectively. In the density distributions, each bar is 3.5 μm wide, and the total number of channels predicted by the model equals the combined areas under all of the bars: 553 (*B*), 612(*D*), and 1336 (*F*). The concentration of cAMP was 10 μM (*A–D*) or 20 μM (*E,F*). Relative residual values (see Methods) were 0.052 (*A*), 0.075 (*C*), and 0.064 (*E*).

voltage led to just a small decrease in the driving force for Na$^+$. In Fig. 6 (recording shown in *black*), the total current decreased from -474 pA to -450 pA over 1 s, reflecting a 5% decrease in the driving force for Na$^+$ into the cilium. This was the largest decrease seen in 11 trials. There was no effect on the driving force for Na$^+$ in the absence of cAMP (Fig. 6, recording shown in *gray*).

Sensitivity analysis

Values treated as constants in the model have been determined experimentally, but most of these are associated with measured experimental errors (Table 2). By using sensitivity analysis, we determined how errors in the constants generated variability in the predictions of the model.

For each of four constants, five values were assumed as described in the legend of Fig. 7. First a density function was generated using the mean value of each constant (Fig. 7 *A*). Then each of 625 permutations of values was used to generate a channel density function. These functions were averaged, and the means and standard errors for the channel

densities at each position in the 625 density functions were calculated (Fig. 7 *B*). There was little variability in the spatial distribution of the channels or in the number of channels reported by the model. Inspection of the 625 individual density functions (not shown) revealed that the primary peak of the density function was at the same position in all cases.

The mathematical model assumes that diffusion of cAMP is limited by binding to sites on the CNG channels. The number of binding sites per channel assumed had only small effects on the channel distribution reported by the model (Fig. 8). Likewise, the channel density functions were similar whether we assumed the proximal ciliary diameter (0.28 μm, Fig. 9 *A*) or the distal diameter (0.19 μm, Fig. 9 *B*). In general, reasonable errors in the constants had little effect on the predicted channel density functions.

Factors that influence the modeled currents

The time course of the predicted current depends very strongly on the assumed channel density function (Fig. 10, *A* and *B*). When the channels are assumed to be near the distal tip of the cilium (Fig. 10, *red*), there are two pronounced
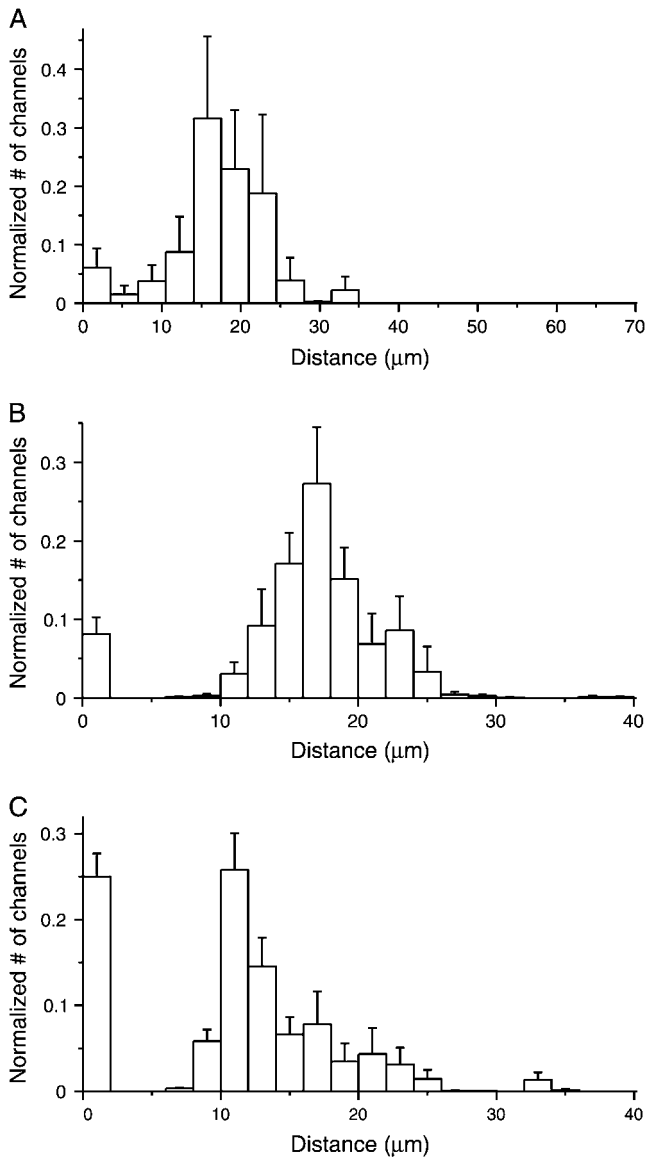
FIGURE 4 Averaged channel density functions generated from multiple experiments in each of three cilia. Average density functions are shown for seven experiments with a 70-μm cilium (A), nine experiments with a 40-μm cilium (B), and eight experiments with a different 40-μm cilium (C). A is from the same 70-μm cilium as in Fig. 3. The model reported the following total numbers of channels: 1148 $\pm$ 172 (A); 565 $\pm$ 45 (B); and 272 $\pm$ 14 (C). Concentrations of cAMP ranged from 1 to 20 μm.

effects. First, the current develops much more slowly than it would with the channels located more proximally. Second, the maximum current amplitude is greatly reduced by cable-conduction loss. Placing the channels away from the base of the cilium also causes a delay in the onset of the current (Fig. 10 B, *black* and *red traces*). There is no delay if channels are present at the base, as is the case with a uniform distribution (Fig. 10 B, *blue*).

Other parameters had smaller effects on the predicted currents. Diffusion of cAMP within the cilium should be
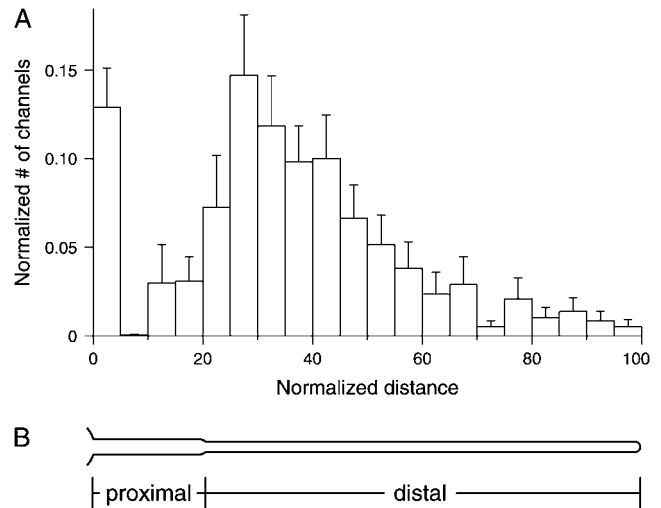

FIGURE 5 (A) CNG channel density function obtained by averaging 42 experiments in 13 different cilia. The lengths of the cilia ranged from 25 to 100 μm. Concentrations of cAMP used ranged from 1 to 20 μM. The model reported the total number of channels to be 1967 $\pm$ 392. (B) Schematic of an olfactory cilium showing the proximal and distal segments, plus a piece of the dendritic knob at the far left. The relative diameters are drawn to scale. The length is scaled to match the distance axis in A.

slowed as cAMP binds to the channels. Thus the time course of the current becomes somewhat slower as the assumed number of binding sites per channel is increased (Fig. 10 C). However, the number of binding sites does not affect the current seen at later times, i.e., after the cAMP solution has
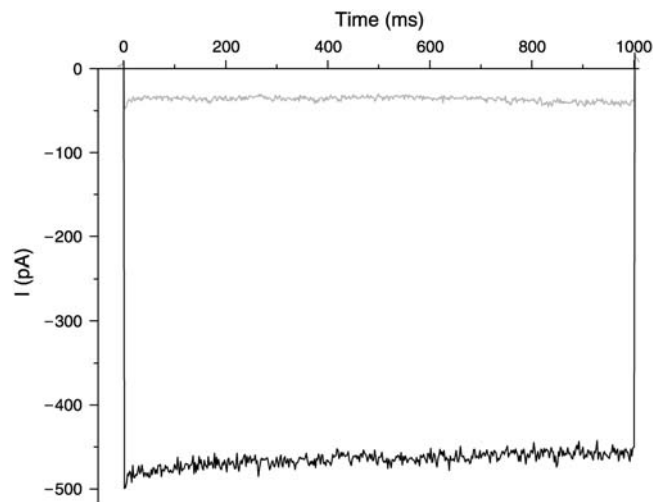

FIGURE 6 Test for a change in driving force during a sustained Na$^+$ current. In the recording shown in black, a cilium was immersed in a bath containing 300 μM cAMP. Voltage was clamped at 0 mV to eliminate any Na$^+$ current. At time 0, the membrane potential was changed to -50 mV. The Na$^+$ current reached a maximum value and then decreased slightly. No change in driving force was detectable when the experiment was repeated in a cAMP-free bath (recording shown in *gray*). For this experiment only, K$^+$-free solutions were used; KCl in the standard solutions was eliminated.

TABLE 2 Constants used in the model

Constant	Value	References
$K_{1/2}$	$1.70 \pm 0.19\ \mu M$ (mean $\pm$ SE)	33
Hill constant, n	1.70 ± 0.07 (mean $\pm$ SE)	Uunpublished data from Kleene (33)
Single-channel conductance, g_{CNG}	8.3 ± 2.3 pS (mean $\pm$ SE)	4
Maximum open probability, P	0.70 ± 0.095 (mean $\pm$ SE)	4
Reversal potential of CNG channel	0 mV	
cAMP binding sites	1/channel	
Ciliary diameter, d	$0.28 \pm 0.03\ \mu m$ (mean $\pm$ SE)	19
cAMP diffusion coefficient, D	3.3×10^{-6} cm^2 s^{-1}	34
Intracellular axial resistance, r_a	1.5×10^{11} Ω cm^{-1}	

Terminology is as in French et al. (17). $K_{1/2}$ is the concentration of cAMP that gives half-maximal activation of the CNG channel. The proximal ciliary diameter is taken from Menco (19), although smaller diameters (proximal $0.22 \pm 0.02\ \mu m$, distal $0.14 \pm 0.03\ \mu m$) have also been reported (22). The diffusion coefficient is the minimum value determined for ATP (34). A similar value (2.7×10^{-6} cm^2 s^{-1}) was measured for cAMP in olfactory receptor neurons (13). The value of r_a corresponds to an intracellular resistivity R_i of 92 Ω cm, i.e., the resistivity of 115 mM NaCl assuming the ciliary diameter shown.

filled the cilium. Decreasing the concentration of cAMP also makes the time course slower, assuming the other parameters are held constant (not shown). By contrast, the assumed ciliary diameter has a greater effect on the current plateau than on the time course (Fig. 10 D). In a cilium of smaller diameter, cable-conduction loss is greater, accounting for the smaller currents.

Varying the number of channels sometimes hastened and sometimes slowed the time course of the current, depending on the other parameters. This is due to a balance of two competing effects: 1), With more channels, there are more total binding sites for cAMP. This slows the diffusion of cAMP and thus tends to slow the time course. 2), With more channels, cable-conduction effects are greater. With large cable effects, the channels nearer the base of the cilium contribute disproportionately to the current. In this case, most of the current is due to a population of channels that are nearer the base and thus activated sooner in our experiments. This tends to hasten the time course of the current. If cable-conduction effects are eliminated from the model, only the first effect remains, and increasing the number of channels always slows the time course.
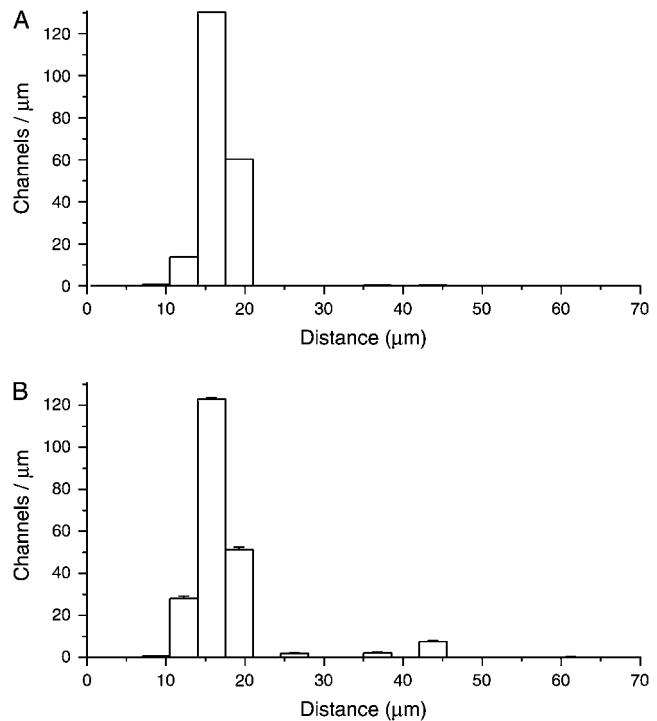
FIGURE 7 Sensitivity analysis of the model. (*A*) A density function was generated by inverse solution from a recording of a single 70-μm cilium placed in 10 μM cAMP. For the constants in the model, the mean values shown in Table 2 were used. The model reported a total of 720 channels. (*B*) Four constants used in the model ($K_{1/2}$ for activation of CNG channels by cAMP, Hill coefficient n, unitary conductance of the CNG channel g_{CNG}, and diffusion coefficient of cAMP D) were varied. A range of values for each of four of the constants was used to generate multiple density functions. For each constant, the maximum and minimum values equaled the mean value plus or minus one standard error or one standard deviation as shown in Table 2. For the diffusion coefficient D, the standard deviation was assumed to be 1×10^{-6} cm^2 s^{-1}. Five values for each constant were used, including the mean, the maximum and minimum values, and two other values equidistant between the maximum and mean or minimum and mean. For the four constants tested, this resulted in $5^4 = 625$ density functions. These 625 density functions were averaged. Mean channel density $\pm$ SE is plotted. The total number of channels reported by the model averaged 752 ± 1 over the 625 density functions.

DISCUSSION

As cAMP diffuses into a cilium, it activates a current with a distinctly biphasic time course (Figs. 2 and 3). Typically there is a short period of time during which little or no current appears, followed by a rapid activation of current. In the simplest case, diffusion time is proportional to the square of the distance diffused. Therefore diffusion over short distances is very much more rapid than diffusion over longer distances. The delay in rapid activation that was often seen probably indicates that there is some distance at the base of the cilium where the channel density is low. The delay should also depend on the mixing time after the cilium is lowered from the air into the bath containing cAMP. However, in some cases this delay was as short as 5 ms; this represents an upper limit of
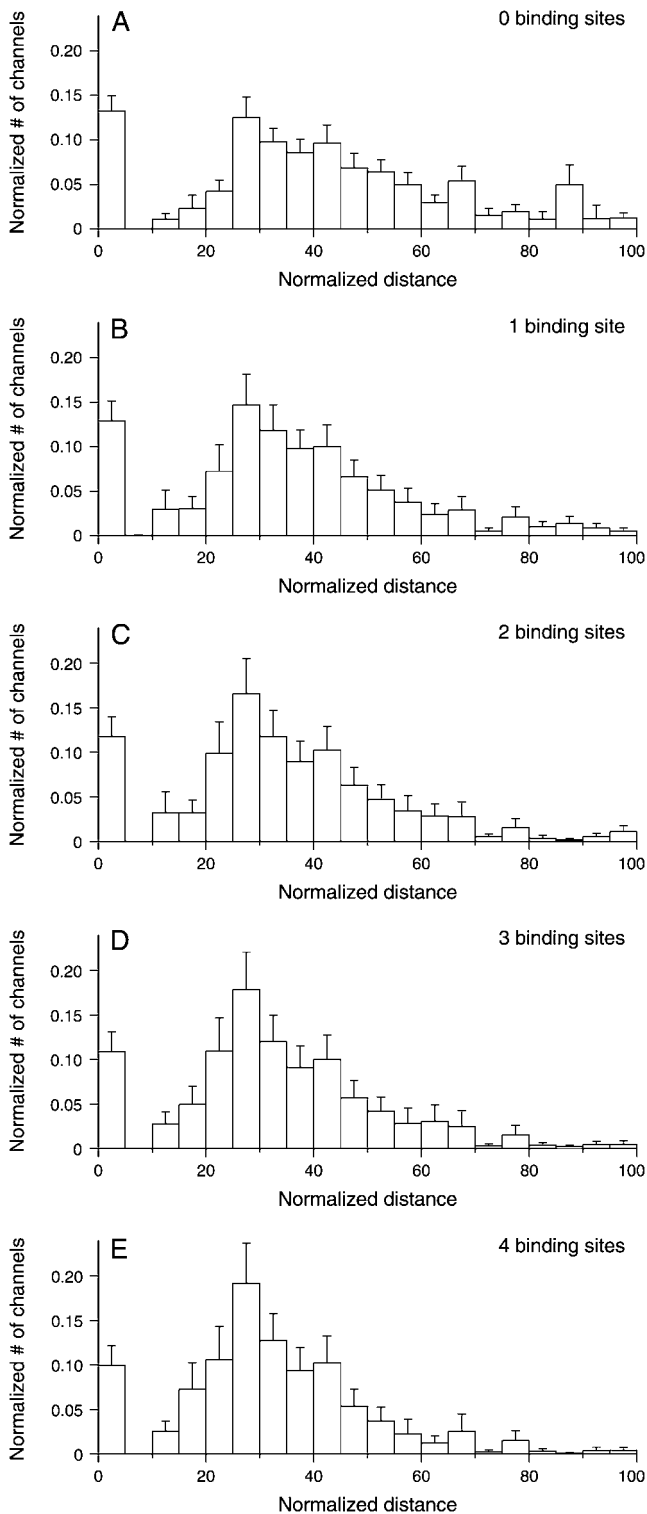
FIGURE 8   Modeled number of cAMP binding sites per CNG channel has little effect on the inferred channel distributions. (A–E) Averaged density functions from 42 experiments in 13 cilia in which each CNG channel was assumed to have 0, 1, 2, 3, or 4 cAMP-binding sites. Concentrations of cAMP used ranged from 1 to 20 μM. The model reported the following total numbers of channels: 2431 $\pm$ 557 (A); 1967 $\pm$ 392 (B); 2612 $\pm$ 556 (C); 3704 $\pm$ 843 (D); and 6099 $\pm$ 1560 (E). B shows the same data as Fig. 5 A.
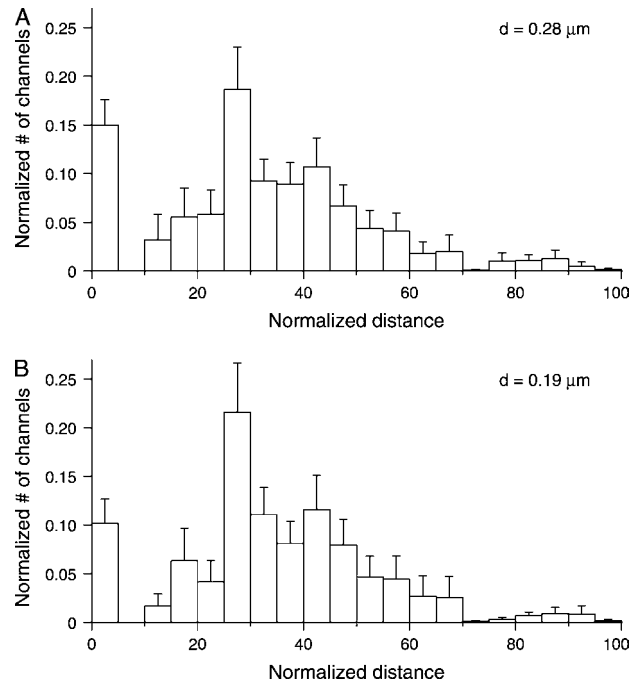

FIGURE 9   Choice of proximal or distal ciliary diameter has little effect on the inferred channel distributions. (A) Averaged density functions from 34 experiments in 8 cilia in which the proximal diameter (0.28 μm) was assumed. (B) Averaged density functions from the same experiments but assuming the distal diameter (0.19 μm). Concentrations of cAMP used ranged from 1 to 20 μM. The model reported the following total numbers of channels: 1195 $\pm$ 238 (A), and 6743 $\pm$ 1156 (B).

the mixing time. The inverse mathematical model uses information from both phases of the recording to generate a channel density function that accounts for the experimental results. Although the results varied among cilia, several trends in channel expression were apparent and were quantified in this study.

The channel distributions can be conveniently discussed by referring to the two ciliary segments defined by morphological studies (Fig. 5 B). In frog, the proximal segment is roughly that 20% of the cilium nearest the cell body (21). The proximal segment has a diameter of 0.28 μm (19), and its axoneme has a full (9 $\times$ 2) + 2 complement of microtubules (19,21). The remaining 80% of the cilium is the distal segment, which has a diameter of 0.19 μm (19). Microtubules in the distal segment are single rather than paired. In the frog the most common configuration is (9 $\times$ 1) + 2, but other arrangements are also common (21,22).

We found that the proximal and distal segments each contain one region with a higher density of CNG channels and a second region with a lower density of channels. The half of the proximal segment nearest the basal body (i.e., the first 10% of the ciliary length) contained on average 13% of the channels (Fig. 5). The channels attributed to this part of the cilium may include some channels from the dendritic knob. It is likely that an excised cilium retains a small portion of the dendritic knob. The dimensions of the pipette tip (diameter
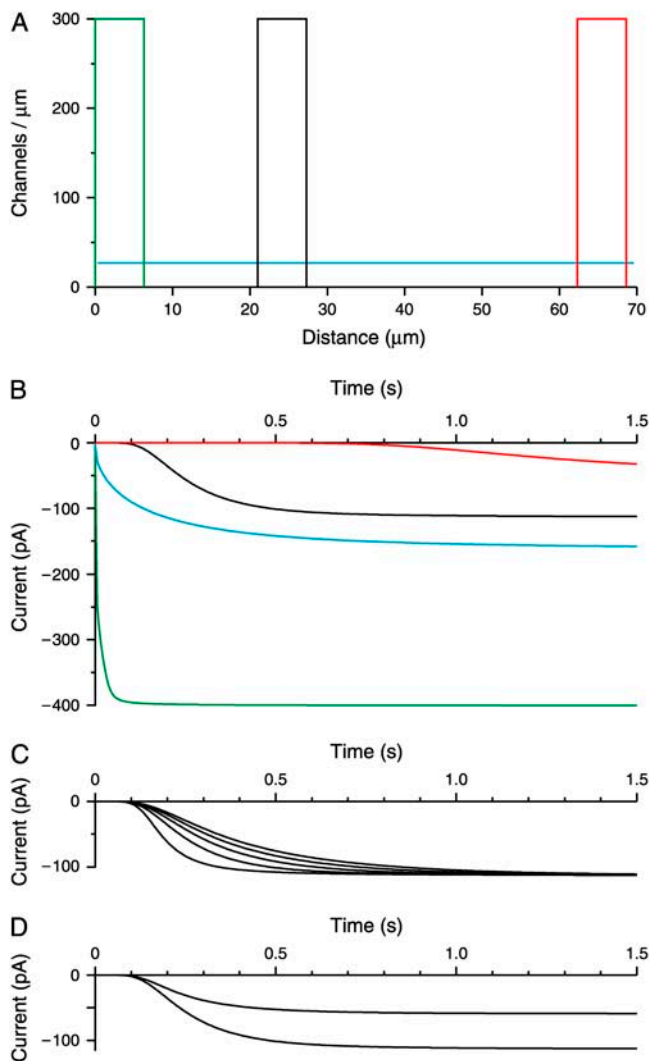
FIGURE 10 Spatial distribution of channels greatly influences the current predicted by the model. (*A*) Four modeled channel distributions. The blue line shows a uniform distribution. The others show narrow bands centered at 3 μm, near the base of the cilium (*green*); 24 μm (*black*); or 65 μm, near the distal tip of the cilium (*red*). The distribution shown in black most closely represents the experimental results (e.g., Fig. 3). In all cases, 1890 channels were placed on a 70-μm cilium. (*B*) The predicted current as a function of time for each of the modeled channel distributions assuming the cilium was placed in a bath containing 20 μM cAMP. Current amplitudes at infinite time were −401 pA (*green*), −161 pA (*blue*), −114 pA (*black*), and −47 pA (*red*). In the absence of cable-conduction loss, the 1890 channels would produce a total current of −541 pA at −50 mV. The smaller plateau values were due to this loss, which is greater as the channels are placed near the distal tip. The times to reach 50% of the plateau current were 8 ms (*green*), 76 ms (*blue*), 252 ms (*black*), and 1.26 s (*red*). (*C*) Effects of varying the assumed number of cAMP-binding sites per channel. From left to right, the predicted currents are shown when 0, 1, 2, 3, or 4 binding sites per channel were assumed. The second curve from the left (one binding site) is the same as the black curve in *B*. Times to reach 50% of the plateau current ranged from 192 to 376 ms. In all cases, the plateau current was −114 pA. (*D*) Effects of assuming a uniform, constant diameter equal to the diameter of the proximal segment (0.28 μm, *lower curve*) or the distal segment (0.19 μm, *higher curve*). The lower curve is the same as the black curve in *B*. Current amplitudes reached −114 pA (0.28 μm) or −59 pA (0.19 μm). Times to reach 50% of the plateau current were 252 ms (0.28 μm) and 243 ms (0.19 μm).

0.5 μm) and the knob (diameter 1–2 μm) determine that the length of dendritic knob contributing to our recordings is <1 μm. Membranes excised from the dendrite do contain some CNG channels, although many more are found in the cilia (6). The remainder of the proximal segment (i.e., the next 10% of the ciliary length) contained 6% of the channels.

The first half of the distal segment (40% of the ciliary length) contained most (69%) of the total CNG channels. The remainder of the distal segment, which is the 40% of the cilium farthest from the basal body, contained just 12% of the channels. In individual cilia (Figs. 3, 4, and 7), the modeled density functions showed very pronounced clustering of channels. Because the peak of channel density varies somewhat from one cilium to the next, density functions from averages of many cilia (Figs. 5, 8, and 9) underrepresent the clustering.

In an earlier electrophysiological study, Lowe and Gold (10) suggested that CNG current-generating capacity might be uniformly distributed along the length of the cilium. Caged cAMP within cilia was photolyzed, and the length of the ciliary bundle illuminated was related to the total current generated. In one neuron, the current was linearly related to the combined ciliary length illuminated, suggesting uniform distribution of channels. However, results from the other four olfactory receptor neurons tested did not support uniform distribution. In all four of those neurons, the cAMP-activated conductance was decreasing or undetectable in the distal half of the ciliary bundle (10). It is now recognized that Lowe and Gold were measuring a sum of currents through both CNG and Ca^{2+}-activated Cl^- channels. The spatial distribution of the Cl^- channels is still unknown.

In a previous study, CNG channel subunit CNGA2 was localized in rat by immunoelectron microscopy (11). The majority of the immunoreactivity was found in the distal segment of the cilium, but it was not determined how channel density varies within the distal segment. (In rat olfactory receptor neurons, the proximal segment is just 2–3 μm in length, whereas the distal segment is 50–60 μm (11).) We have now shown that channel expression is concentrated in a band of the distal segment and demonstrated that these distal channels are functional.

We used an inverse solution of a mathematical model to infer the spatial distribution of the CNG channels. Part of the solution process has a very high condition number, suggesting that other channel distributions could account for the experimental result. In other words, it is theoretically possible that other density functions, when used as input to the forward biophysical model, could produce the same predicted current. However, previous investigations with sample channel distributions suggest that this is rarely the case (17). This study demonstrates that although there may be many solutions, these solutions have both qualitative and quantitative features that are highly reproducible. These features include: 1), a short region in the proximal segment where no functional channels exist, 2), a short region in the distal segment that contains the majority of the channels, and

3), a larger region at the distal end that has few functional channels. Other features were moderately to highly variable. These features include the total number of channels and the appearance of minor clusters of channels in very distal regions. Modeled predictions of the number of channels in far distal regions were expected to be somewhat variable due to the broadening of the cAMP concentration profile at that distance and the smaller currents from the distal channels due to cable-conduction loss. For these reasons, the model is not as sensitive to small changes in channel densities in the far distal regions.

Nine experimentally determined values were treated as constants in the model (Table 2), but most of these values were associated with measured experimental errors. Sensitivity analysis of six of these constants (Figs. 7–9) revealed that the channel density function was only mildly dependent on reasonable changes in the constants. We would not have predicted this in all cases. It was surprising, for example, that binding of cAMP to the CNG channels had little effect on the inferred channel distributions (Fig. 8). A model 50-μm cilium filled with 10 μM cAMP should contain ~14,000 molecules of cAMP. If a cilium has 2500 CNG channels (3), each with four cAMP-binding sites (23), diffusion of cAMP should be significantly slowed by this binding. The forward model shows that such a dependence exists but is modest for a typical cilium (Fig. 10 C). Neither this binding nor the assumed ciliary diameter (Fig. 9) strongly influenced the channel distributions reported by the model. A much stronger relation exists between the time course of the current and the locations of the channels along the ciliary length (Fig. 10). As a result, the model allows the channel distribution to be inferred from the current recording. It is also notable that the channel locations and ciliary diameter strongly affect the current amplitude (Fig. 10) and should thus be important determinants of neuronal sensitivity.

It is not clear yet why functional channels are rare in the most distal 40% of the cilium. In chemosensory cilia of *Caenorhabditis elegans*, intraflagellar transport (IFT) is required for expression of some transduction channels in the distal segment (24). The distal segment of the frog cilium has an incomplete axoneme (21), and one could imagine that this prevents the CNG channels from being transported toward the distal tip. However, two facts make this explanation unlikely. First, on average the highest density of CNG channels was found 28% down the length of the cilium (Fig. 5). This is already within the distal segment, assuming the distal segment is 80% of the ciliary length (21). Second, IFT of axonemal components occurs even in distal ciliary segments where the axoneme is composed of singlet tubules (25). It is possible that channels in the farthest distal regions of cilia lose their functionality because they are exposed to a relatively unregulated external environment. As viewed by freeze-fracture electron microscopy, the distal tips of frog olfactory cilia display a high density of intramembrane particles (26). However, it is not known whether these particles include functional channels.

Channel clustering is a phenomenon observed in many cell types and neuronal compartments, including neuronal axons, hair cells of the inner ear (27), skeletal myotubes (28), and pancreatic β cells (29). The functions of channel clustering include regulation of oscillation frequency in hair cells and neurosecretory cells, as well as compartmentalization of signaling components in neuronal synapses. In olfactory cilia, clustering of CNG channels may be part of a system that enhances the efficiency of signal transduction. Odor transduction in cilia is initiated by an odor molecule binding to a G-protein-coupled receptor, which results in the formation of cAMP. cAMP then activates the CNG channels, and Ca^{2+} entering through the CNG channels gates Ca^{2+}-activated Cl^- channels (reviewed in Schild and Restrepo (1)). A concentration of these components should enhance the efficiency of transduction. For example, cAMP may be hydrolyzed by a phosphodiesterase before it diffuses to a CNG channel. If the site of cAMP synthesis is close to a channel, channel activation may be favored over cAMP hydrolysis. Concentration of transduction components could also facilitate the amplifying function of the Cl^- channels. Intracellular Ca^{2+} concentration is expected to reach higher values near Ca^{2+} channel clusters (30) such as the CNG channel clusters we observed. A higher Ca^{2+} concentration should result in greater activation of Cl^- channels. The higher concentration of Ca^{2+} that results from CNG channel clustering will result in a higher ratio of Cl^-/CNG channel activity, which is optimal for maximizing the signal/noise ratio of the receptor current (3). Although most of the molecules of olfactory transduction are concentrated in the distal segment of the cilium (2), it is not known if they are particularly localized to the smaller domain where the CNG channels are clustered. Transduction could be improved by grossly concentrating the proteins within such a 10- to 15-μm length of the cilium. Furthermore, the proteins may be concentrated at the molecular level within microdomains (31,32).

REFERENCES

1. Schild, D., and D. Restrepo. 1998. Transduction mechanisms in vertebrate olfactory receptor cells. *Physiol. Rev.* 78:429–466.

2. Menco, B. Ph. M. 1997. Ultrastructural aspects of olfactory signaling. *Chem. Senses.* 22:295–311.

3. Kleene, S. J. 1997. High-gain, low-noise amplification in olfactory transduction. *Biophys. J.* 73:1110–1117.

4. Larsson, H. P., S. J. Kleene, and H. Lecar. 1997. Noise analysis of ion channels in non-space-clamped cables: estimates of channel parameters in olfactory cilia. *Biophys. J.* 72:1193–1203.

5. Kleene, S. J., R. C. Gesteland, and S. H. Bryant. 1994. An electrophysiological survey of frog olfactory cilia. *J. Exp. Biol.* 195:307–328.

6. Kurahashi, T., and A. Kaneko. 1993. Gating properties of the cAMP-gated channel in toad olfactory cells. *J. Physiol.* 466:287–302.

7. Lindemann, B. 2001. Predicted profiles of ion concentrations in olfactory cilia in the steady state. *Biophys. J.* 80:1712–1721.

8. Karpen, J. W., and T. C. Rich. 2004. Resolution of cAMP signals in three-dimensional microdomains using novel, real-time sensors. *Proc. West. Pharmacol. Soc.* 47:1–5.

9. Karpen, J. W., and T. C. Rich. 2005. High-resolution measurements of cyclic adenosine monophosphate signals in 3D microdomains. *Methods Mol. Biol.* 307:15–26.

10. Lowe, G., and G. H. Gold. 1993. Contribution of the ciliary cyclic nucleotide-gated conductance to olfactory transduction in the salamander. *J. Physiol.* 462:175–196.

11. Matsuzaki, O., R. E. Bakin, X. Cai, B. Ph. M. Menco, and G. V. Ronnett. 1999. Localization of the olfactory cyclic nucleotide-gated channel subunit 1 in normal, embryonic and regenerating olfactory epithelium. *Neuroscience.* 94:131–140.

12. Reisert, J., P. J. Bauer, K.-W. Yau, and S. Frings. 2003. The Ca-activated Cl channel and its control in rat olfactory receptor neurons. *J. Gen. Physiol.* 122:349–363.

13. Chen, C., T. Nakamura, and Y. Koutalos. 1991. Cyclic AMP diffusion coefficient in frog olfactory cilia. *Biophys. J.* 76:2861–2867.

14. Kleene, S. J., and R. C. Gesteland. 1991. Transmembrane currents in frog olfactory cilia. *J. Membr. Biol.* 120:75–81.

15. Kleene, S. J. 1993. Origin of the chloride current in olfactory transduction. *Neuron.* 11:123–132.

16. Kurahashi, T., and K.-W. Yau. 1993. Co-existence of cationic and chloride components in odorant-induced current of vertebrate olfactory receptor cells. *Nature.* 363:71–74.

17. French, D. A., R. J. Flannery, C. W. Groetsch, W. B. Krantz, and S. J. Kleene. 2006. Numerical approximation of solutions of a nonlinear inverse problem arising in olfaction experimentation. *Math. Comput. Model.* 43:945–956.

18. Kleene, S. J. 1992. Basal conductance of frog olfactory cilia. *Pflugers Arch.* 421:374–380.

19. Menco, B. Ph. M. 1980. Qualitative and quantitative freeze-fracture studies on olfactory and nasal respiratory structures of frog, ox, rat, and dog. *Cell Tissue Res.* 207:183–209.

20. Zimmerman, A. L., J. W. Karpen, and D. A. Baylor. 1988. Hindered diffusion in excised membrane patches from retinal rod outer segments. *Biophys. J.* 54:351–355.

21. Reese, T. S. 1965. Olfactory cilia in the frog. *J. Cell Biol.* 25:209–230.

22. Lidow, M. S., and B. Ph. M. Menco. 1984. Observations on axonemes and membranes of olfactory and respiratory cilia in frogs and rats using tannic acid-supplemented fixation and photographic rotation. *J. Ultrastruct. Res.* 86:18–30.

23. Kaupp, U. B., and R. Seifert. 2002. Cyclic nucleotide-gated ion channels. *Physiol. Rev.* 82:769–824.

24. Qin, H., D. T. Burnette, Y.-K. Bae, P. Forscher, M. M. Barr, and J. L. Rosenbaum. 2005. Intraflagellar transport is required for the vectorial movement of TRPV channels in the ciliary membrane. *Curr. Biol.* 15:1695–1699.

25. Snow, J. J., G. Ou, A. L. Gunnarson, M. R. Walker, H. M. Zhou, I. Brust-Mascher, and J. M. Scholey. 2004. Two anterograde intraflagellar transport motors cooperate to build sensory cilia on *C. elegans* neurons. *Nat. Cell Biol.* 6:1109–1113.

26. Menco, B. Ph. M. 1992. Ultrastructural studies on membrane, cytoskeletal, mucous, and protective compartments in olfaction. *Microsc. Res. Tech.* 22:215–224.

27. Rispoli, G., M. Martini, M. L. Rossi, and F. Mammano. 2001. Dynamics of intracellular calcium in hair cells isolated from the semicircular canal of the frog. *Cell Calcium.* 30:131–140.

28. Anson, B. D., and W. M. Roberts. 2002. Sodium channel distribution on uninnervated and innervated embryonic skeletal myotubes. *J. Neurobiol.* 48:42–57.

29. Johnson, J. D., S. Kuang, S. Misler, and K. S. Polonsky. 2004. Ryanodine receptors in human pancreatic beta cells: localization and effects on insulin secretion. *FASEB J.* 18:878–880.

30. Shuai, J. W., and P. Jung. 2002. Optimal intracellular calcium signaling. *Phys. Rev. Lett.* 88:068102.

31. Paysan, J., and H. Breer. 2001. Molecular physiology of odor detection: current views. *Pflugers Arch.* 441:579–586.

32. Brady, J. D., T. C. Rich, X. Le, K. Stafford, C. J. Fowler, L. Lynch, J. W. Karpen, R. L. Brown, and J. R. Martens. 2004. Functional role of lipid raft microdomains in cyclic nucleotide-gated channel activation. *Mol. Pharmacol.* 65:503–511.

33. Kleene, S. J. 1999. Both external and internal calcium reduce the sensitivity of the olfactory cyclic-nucleotide-gated channel to cAMP. *J. Neurophysiol.* 81:2675–2682.

34. Bowen, W. J., and H. L. Martin. 1964. The diffusion of adenosine triphosphate through aqueous solutions. *Arch. Biochem. Biophys.* 107:30–36.